Journal of Sound and Vibration 329 (2010) 3417–3430

Contents lists available at ScienceDirect

Journal of Sound and Vibration

journal homepage: www.elsevier.com/locate/jsvi

A six-axis hybrid vibration isolation system using active zero-power control supported by passive weight support mechanism

Md. Emdadul Hoque *, Takeshi Mizuno, Yuji Ishino, Masaya Takasaki

Department of Mechanical Engineering, Saitama University, 255 Shimo-Okubo, Sakura-Ku, Saitama 338-8570, Japan

ARTICLE INFO

Article history:
Received 14 October 2009
Received in revised form
1 March 2010
Accepted 4 March 2010
Handling Editor: J. Lam

ABSTRACT

This paper presents a six-degree-of-freedom hybrid vibration isolation system integrated with an active negative suspension, an active–passive positive suspension and a passive weight support mechanism. The aim of the research consists in maximizing the system and control performances, and minimizing the system development and maintenance costs. The vibration isolation system is, fundamentally, developed by connecting an active negative suspension realized by zero-power control in series with an active–passive positive suspension. The system could effectively isolate ground vibrations in addition to suppress the effect of on-board generated direct disturbances of the six-axis motions, associated with vertical and horizontal directions. The system is further reinforced by introducing a passive weight support mechanism in parallel with the basic system. The modified system with zero-power control allows simplified design of the isolation table without power consumption. It also offers enhanced performance on direct disturbance suppression and large payload supporting capabilities, without degrading transmissibility characteristics. A mathematical model of the system is presented and, therefore, analyzed to demonstrate that zero-compliance to direct disturbance could be generated by the developed system. Experimental demonstrations validate the proposed concept that exhibits high stiffness of the isolation table to static and dynamic direct disturbances, and good transmissibility characteristics against ground vibration. Further improvements of the vibration isolation system and the control system are discussed as well.

1. Introduction

Vibration isolation and control have become a widespread and significant challenge in many advanced fields including semiconductor manufacturing, precision measurement, space vehicle and many other applications. Vibrations of mechanical systems are usually dealt with passive damping and passive isolation. Passive techniques are effectively used in many applications; however, those are associated with undeniable limitations for the trade-off, because the isolation elements need to be soft enough to reduce the transmission of ground vibration and stiff enough to prevent on-board generated direct disturbances [1,2]. On the contrary, conventional active system can be an adequate substitute to avoid the trade-off [3–11]. Benassi et al. [4] developed an active isolation system using force feedback control, Yasuda et al. [5] proposed an active system to control a two-degree-of-freedom system, and Yoshioka et al. [6] presented a six-axis system with absolute displacement and velocity feedback by accelerometer. Different control approaches are also used to

* Corresponding author. Tel.: +81 48 858 3453; fax: +81 48 858 3712.
E-mail addresses: mehoque@mech.saitama-u.ac.jp, emdad89@yahoo.com (Md. Emdadul Hoque).

0022-460X/$ - see front matter © 2010 Elsevier Ltd. All rights reserved.
doi:10.1016/j.jsv.2010.03.003

develop vibration isolation system, such as feedforward control by Yasuda et al. [7], H^{∞} control by Watanabe et al. [8], repetitive control by Daley et al. [9] and an active acceleration control by Zhu et al. [10]. However, most of the conventional active systems use high-performance sensors such as servo-type accelerometers for acceleration feedback to detect the vibration of an isolation table in a low frequency region and also use external power supply for stable operation. Therefore, the system becomes rather costlier than the passive-type system. Sato and Trumper [11] developed an isolator by connecting an active negative spring in parallel with a positive spring that achieved good vibration isolation performance and platform releveling by position and velocity control of the platform. However, excessive heat was generated in the actuator caused by drive currents and much power was consumed by the system. The authors have proposed a unique vibration isolation system using active zero-power magnetic suspension to overcome the above shortcomings [12–14]. The proposed vibration isolation system uses only relative displacement feedback by eddy current displacement sensors, which is much cheaper than servo-type accelerometers. The control current of the zero-power system converges to zero during its stable operation and, thus, saves the energy. Due to its power saving characteristics, zero-power control can be used in vibration isolation system [14], carrier system in clean room [15] and momentum wheels for spacecraft stabilization [16].

Zero-power control system is realized by using hybrid magnet consisting of a permanent magnet for providing bias flux and an electromagnet for stabilization [17]. The electromagnet is controlled for the steady deviation of the coil current to converge to zero. Therefore, the permanent magnet balances the suspended object, and maintains a nominal air gap length. A unique characteristic of the zero-power control system is that it behaves as if it has negative stiffness; when an external force is applied to the suspended object, the suspended object moves to a new equilibrium position located in the direction opposite to the applied force. Since a zero-power system behaves as if it has negative stiffness, an infinite stiffness against disturbances on the isolation table can be achieved by combining it with a mechanical spring of equal stiffness. It enables the system to have good characteristics both in reducing vibration transmitted from the floor and in suppressing direct disturbances.

In such a system, however, the ability of the isolation table to support payload on the table is limited to the capacity of the permanent magnets in the basic system. Therefore, the system is modified furthermore adding passive weight support mechanism between the isolation table and the base in parallel with the basic system presented by Hoque et al. [14]. The concept of the weight support mechanism is introduced analytically for further investigation [18], and a single-axis apparatus was manufactured for basic experimental study [19]. Finally, a six-axis apparatus was fabricated, and some preliminary results with basic analytical study of a single-degree-of-freedom model are presented [20].

This paper focuses on the development of a six-axis vibration isolation system showing detailed relations between the isolation table and middle table and the middle table and the base, and on the control of its vertical and horizontal motions using hybrid active and passive techniques. The structure of the paper is organized as follows: the motivation of research for developing vibration isolation system using hybrid technique is introduced in Section 1. In Section 2, the basic concept and configuration of the vibration isolation system is described. Next, a mathematical model of the developed system is derived, and it is analyzed that the developed system has theoretically infinite stiffness or zero-compliance to direct disturbances. Section 4 explains the control system design. Section 5 demonstrates the experimental results to verify the efficacy of the proposed control system. Finally, conclusions are made on the developed system as well as control technique, and further improvements are discussed as well.

2. Outline of the vibration isolation system

2.1. Vibration isolation technique supported by weight support mechanism

The design of vibration isolation technique is based on the concept that it can deal with two kinds of vibrations; one is on-board generated direct disturbance or vibration caused by direct disturbance on the isolation table, and another one is ground vibrations. In the previous research, the vibration isolation system was developed to generate infinite stiffness by connecting a mechanical spring in series with a magnetic spring that has negative stiffness. The negative stiffness is realized by an active zero-power control [14]. The concept is modified by introducing a secondary suspension, k_3, as demonstrated in Fig. 1, in parallel with the basic system to avoid some limitations that the previous system (presented in [14]) suffered during system design and supporting heavy payloads [20]. The total stiffness k_c of such a modified system is given by

$$k_c = \frac{k_1 k_2}{k_1 + k_2} + k_3. \tag{1}$$

However, if one of the springs has negative stiffness (using zero-power control) that satisfies $k_1 = -k_2$, the resultant stiffness becomes infinite for any finite value of k_3, that is

$$|k_c| = \infty. \tag{2}$$

Therefore, the proposed system can generate zero-compliance (theoretically infinite stiffness) against direct disturbance on the isolation table. On the other hand, it can maintain suitable ground vibration isolation performance as well, if low stiffness of mechanical springs (k_1, k_3) is used in the lower part.

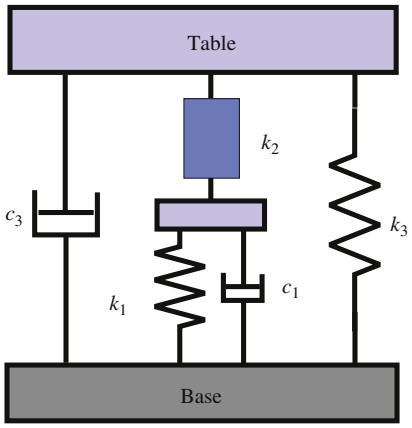

Fig. 1. Basic structure of vibration isolation system. k_1 is normal spring, k_2 is the active negative spring (zero-power control) and k_3 is the passive weight support mechanism.

2.2. Zero-power control system

The negative stiffness, as mentioned in Section 2.1, can be realized either by passive [21] or active approach [12]. Systems containing passive elements with negative stiffness are generally unstable because they generate force in the direction opposite to restoring, and additionally, passive system has some limitations in suppressing both disturbances. Active control is necessary to realize negative stiffness without instability and, therefore, used in this research. The active zero-power control is achieved by using hybrid magnet, which consists of electromagnet and permanent magnets. There is no steady energy consumption for achieving stable levitation. It is to be mentioned that the power supply must be operated even in the steady states to continue stabilization by active control.

A minimal order compensator achieving zero-power control, and assigning the closed-loop poles arbitrarily can be represented as [17]

$$I(s) = -\frac{s(\tilde{h}_2 s + \tilde{h}_1)}{s^2 + g_1 s + g_0} X(s). \tag{3}$$

In such a case, the characteristic polynomial of the closed-loop system is obtained as [17]

$$t_c(s) = s^4 + g_1 s^3 + (-a_0 + g_0 + b_0 \tilde{h}_2) s^2 + (-a_0 g_1 + b_0 \tilde{h}_1) s - a_0 g_0. \tag{4}$$

Assuming that the characteristic polynomial specifying the desired location of the roots is

$$t_d(s) = (s^2 + 2\zeta_1 \omega_1 s + \omega_1^2)(s^2 + 2\zeta_2 \omega_2 s + \omega_2^2). \tag{5}$$

The coefficients of g_i's and h_i's of the controller of Eq. (3) are determined uniquely by comparing the coefficients in Eqs. (4) and (5). The details of the zero-power control system with realization of zero-power control current and achieving negative stiffness are presented in [17].

2.3. Development of the six-axis system

The vibration isolation system was developed based on the principle discussed in Eq. (1). Fig. 2 depicts the six-axis hybrid vibration isolation system with weight support springs [20]. It consisted of a rectangular isolation table, a middle table and base. A positive stiffness suspension realized by electromagnet and normal springs was used between the base and the middle table. On the other hand, a negative stiffness suspension generated by hybrid magnets was used between the middle table and isolation table. The height, length, width and mass of the apparatus were 300 mm, 740 mm, 590 mm and 400 kg, respectively. The isolation and middle tables weighed 88 and 158 kg, respectively. The isolation table had six-degree-of-freedom motions in the x, y, z, roll, pitch and yaw directions.

The base was equipped with four pairs of coil springs and electromagnets (actively controlled) to support the middle table in the vertical direction and six pairs of coil springs and electromagnets (two pairs in the x-direction and four pairs in the y-direction) in the horizontal directions. The middle table was equipped with four sets of hybrid magnets to levitate and control the motions of the isolation table in the vertical direction and six sets of hybrid magnets (two sets in the x-direction and four sets in the y-direction) to control the motions of the table in the horizontal directions. The isolation table was also supported by four coil springs in the vertical direction and six coil springs (two in the x-direction and four in the y-direction) in the horizontal directions as weight support mechanism. Each set of hybrid magnet for zero-power suspension consisted of five square-shaped permanent magnets (20 mm × 20 mm × 2 mm) and five 585-turn electromagnets. The two-pole permanent magnet is made of NdFeB materials. The spring constant of each normal spring

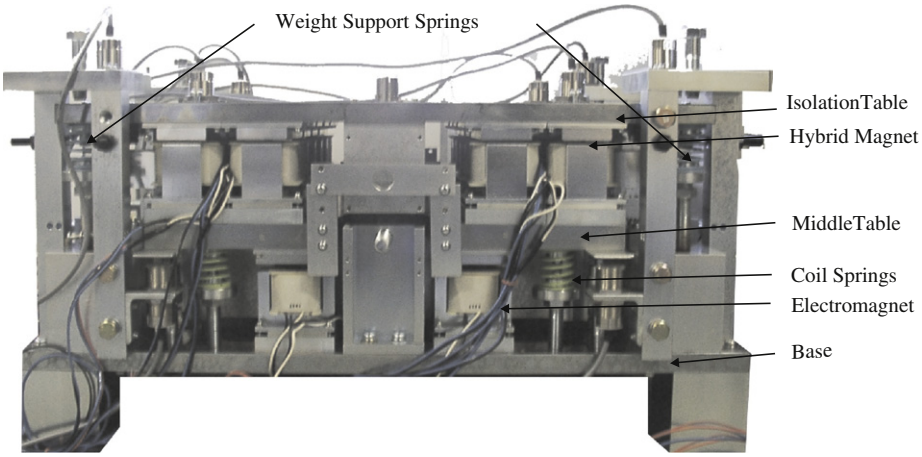

Fig. 2. Photograph of the developed six-axis vibration isolation system.

was 12.1 N/mm and that of weight support spring was 25.5 N/mm. There was flexibility to change the position of the weight support springs (both in the vertical and horizontal directions) to make it compatible for designing stable magnetic suspension system using zero-power control.

The relative displacements of the isolation table to the middle table and those of the middle table to the base were detected by eight eddy current displacement sensors, provided by Swiss-made Baumer electric, attached to the corners of the isolation table and the base. Similarly six pairs of sensors were used to measure the relative displacement between the middle table and the base. To measure the displacement of the isolation table with respect to base, four additional sensors were placed at the base attachments. Those sensors were solely utilized for measurement purposes.

3. Mathematical model of the system and analysis

3.1. Basic model of the system

The developed six-axis motion of the isolation system with weight support spring will be treated analytically in this section. The schematic diagram of the isolation table and the middle table with the coordinate system is shown in Fig. 3. The equation of motion of the isolation table in the vertical direction can be written as

$$\mathbf{M_v}\begin{bmatrix}\ddot{z}\\ \ddot{\theta}_x\\ \ddot{\theta}_y\end{bmatrix} = -\begin{bmatrix}f_z^e\\ m_x^e\\ m_y^e\end{bmatrix} + \begin{bmatrix}f_z^d\\ m_x^d\\ m_y^d\end{bmatrix} + \begin{bmatrix}f_z^W\\ m_x^W\\ m_y^W\end{bmatrix}, \tag{6}$$

where

$$\mathbf{M_v} = \begin{bmatrix}m & 0 & 0\\ 0 & J_x & 0\\ 0 & 0 & J_y\end{bmatrix}, \tag{7}$$

m is the mass of the isolation table, J_x the moment of inertia of the isolation table about x-axis, J_y the moment of inertia of the isolation table about y-axis, z the z-direction displacement of the center of the isolation table, f_z^e the z-direction total force by the hybrid magnets, m_x^e the total moment about x-axis by the hybrid magnets, m_y^e the total moment about y-axis by the hybrid magnets, f_z^d the z-direction direct disturbance, m_x^d the direct disturbance about x-axis, m_y^d the direct disturbance about y-axis, f_z^W the z-direction total weight support force, m_x^W the total moment about x-axis by weight support force, m_y^W the total moment about y-axis by weight support force, and θ_x, θ_y are, respectively, the roll and pitch angles of the isolation table.

The equation of motion of the middle table can be written as

$$\overline{\mathbf{M}}_\mathbf{v}\begin{bmatrix}\ddot{\bar{z}}\\ \ddot{\bar{\theta}}_x\\ \ddot{\bar{\theta}}_y\end{bmatrix} = \begin{bmatrix}f_z^e\\ m_x^e\\ m_y^e\end{bmatrix} + \begin{bmatrix}f_z^p\\ m_x^p\\ m_y^p\end{bmatrix}, \tag{8}$$

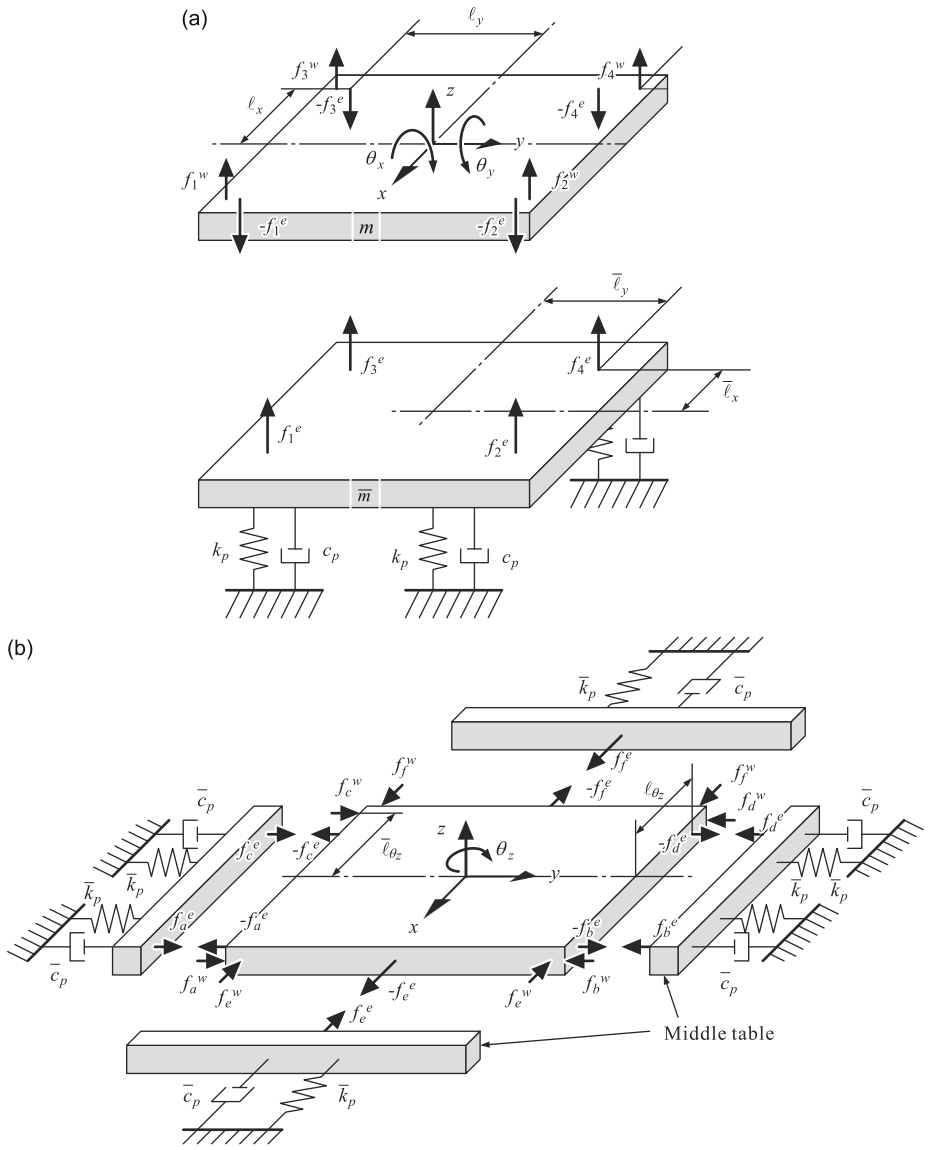

Fig. 3. Coordinate system for six-axis motions of the isolation table and middle table: (a) motion in the vertical direction and (b) motion in the horizontal directions.

where

$$\overline{\mathbf{M}}_{\mathbf{v}} = \begin{bmatrix} \overline{m} & 0 & 0 \\ 0 & \overline{J}_x & 0 \\ 0 & 0 & \overline{J}_y \end{bmatrix}, \tag{9}$$

$\overline{m}$ is the mass of the middle table, $\overline{J}_x$ the moment of inertia of the middle table about x-axis, $\overline{J}_y$ the moment of inertia of the middle table about y-axis, $\overline{z}$ the z-direction displacement of the center of the middle table, f_z^p the z-direction total force by the springs and dampers, m_x^p the total moment about x-axis by the springs and dampers, m_y^p the total moment about y-axis by the springs and dampers, and $\overline{\theta}_x$, $\overline{\theta}_y$ are, respectively, the pitch and roll angles of the middle table.

The total forces and torques are related to the forces generated by the hybrid magnets as

$$\begin{bmatrix} f_z^e \\ m_x^e \\ m_y^e \end{bmatrix} = \mathbf{R}_{\mathbf{a}} \begin{bmatrix} f_1^e \\ f_2^e \\ f_3^e \end{bmatrix}, \tag{10}$$

$$\mathbf{R_a} = \begin{bmatrix} 1 & 1 & 1 & 1 \\ l_y & -l_y & l_y & -l_y \\ l_x & l_x & -l_x & -l_x \end{bmatrix}, \tag{11}$$

where f_u^e is the attractive force of the hybrid magnet u (u=1, 2, 3). The force of each magnet is approximately given by $f_u^e = -k_s r_u + k_i i_u$, where r_u is the deviation of the gap between the electromagnets and the targets on the isolation table, and i_u is the control current.

The gaps are related to the displacements as

$$\begin{bmatrix} r_1 \\ r_2 \\ r_3 \end{bmatrix} = \mathbf{R_b} \begin{bmatrix} \overline{z} \\ \overline{\theta}_x \\ \overline{\theta}_y \end{bmatrix} - \begin{bmatrix} z \\ \theta_x \\ \theta_y \end{bmatrix}, \tag{12}$$

$$\mathbf{R_b} = \begin{bmatrix} 1 & l_y & l_x \\ 1 & -l_y & l_x \\ 1 & l_y & -l_x \\ 1 & -l_y & -l_x \end{bmatrix}. \tag{13}$$

The total forces and torques by the springs and dampers are given by

$$\begin{bmatrix} f_z^p \\ m_x^p \\ m_x^p \end{bmatrix} = \mathbf{R_a} \begin{bmatrix} f_1^p \\ f_2^p \\ f_3^p \end{bmatrix} = \mathbf{R_a} \left(k_p + c_p \frac{\mathrm{d}}{\mathrm{d}t} \right) \left(\begin{bmatrix} \hat{z}_1 \\ \hat{z}_2 \\ \hat{z}_3 \end{bmatrix} - \mathbf{R_b} \begin{bmatrix} \overline{z} \\ \overline{\theta}_x \\ \overline{\theta}_y \end{bmatrix} \right), \tag{14}$$

where $\hat{z}_u$ is the displacement of the base at the position u, k_p the stiffness of the spring in the vertical direction, and c_p the damping constant of the damper in the vertical direction.

The equation of motion of the isolation table in the horizontal directions can be written as

$$\mathbf{M_h} \begin{bmatrix} \ddot{x} \\ \ddot{y} \\ \ddot{\theta}_z \end{bmatrix} = - \begin{bmatrix} f_x^e \\ f_y^e \\ m_z^e \end{bmatrix} + \begin{bmatrix} f_x^d \\ f_y^d \\ m_z^d \end{bmatrix} + \begin{bmatrix} f_x^W \\ f_y^W \\ m_z^W \end{bmatrix}, \tag{15}$$

where

$$\mathbf{M_h} = \begin{bmatrix} m & 0 & 0 \\ 0 & m & 0 \\ 0 & 0 & J_z \end{bmatrix}, \tag{16}$$

J_z is the moment of inertia of the isolation table about z-axis, x the x-direction displacement of the center of the isolation table, y the y-direction displacement of the center of the isolation table, f_x^e the x-direction total force by the hybrid magnets, f_y^e the y-direction total force by the hybrid magnets, m_z^e the total moment about z-axis by the hybrid magnets, f_x^d the x-direction direct disturbance, f_y^d the y-direction direct disturbance, m_z^d the direct disturbance about z-axis, f_x^W the x-direction total weight support force, f_y^W the y-direction total weight support force, m_z^W the total moment about z-axis by weight support force, and θ_z the yaw angle of the isolation table.

The equation of motion of the middle table in the horizontal directions can be written as

$$\overline{\mathbf{M}}_\mathbf{h} \begin{bmatrix} \ddot{\overline{x}} \\ \ddot{\overline{y}} \\ \ddot{\overline{\theta}}_z \end{bmatrix} = \begin{bmatrix} f_x^e \\ f_y^e \\ m_z^e \end{bmatrix} + \begin{bmatrix} f_x^p \\ f_y^p \\ m_z^p \end{bmatrix}, \tag{17}$$

where

$$\overline{\mathbf{M}}_\mathbf{h} = \begin{bmatrix} \overline{m} & 0 & 0 \\ 0 & \overline{m} & 0 \\ 0 & 0 & \overline{J}_z \end{bmatrix}, \tag{18}$$

$\overline{J}_z$ is the moment of inertia of the middle table about z-axis, $\overline{x}$ the x-direction displacement of the center of the middle table, $\overline{y}$ the y-direction displacement of the center of the middle table, f_x^p the x-direction total force by the springs and dampers, f_y^p the y-direction total force by the springs and dampers, m_z^p the total moment about z-axis by the springs and dampers, and $\overline{\theta}_z$ the yaw angle of the middle table.

The total forces and torques are related to the forces generated by the hybrid magnets as

$$\begin{bmatrix} f_x^e \\ f_y^e \\ m_z^e \end{bmatrix} = \overline{\mathbf{R}}_\mathbf{a} \begin{bmatrix} f_4^e \\ f_5^e \\ f_6^e \end{bmatrix} = \begin{bmatrix} 1 & -1 & 1 & -1 & 0 & 0 \\ 0 & 0 & 0 & 0 & 1 & -1 \\ l_z & -l_z & l_z & -l_z & 0 & 0 \end{bmatrix} \begin{bmatrix} f_4^e \\ f_5^e \\ f_6^e \end{bmatrix}. \tag{19}$$

The gaps are related to the displacements as

$$\begin{bmatrix} r_4 \\ r_5 \\ r_6 \end{bmatrix} = \overline{\mathbf{R}}_\mathbf{b} \left(\begin{bmatrix} \overline{x} \\ \overline{y} \\ \overline{\theta}_z \end{bmatrix} - \begin{bmatrix} x \\ y \\ \theta_z \end{bmatrix} \right), \tag{20}$$

$$\overline{\mathbf{R}}_\mathbf{b} = \begin{bmatrix} 1 & 0 & l_z \\ -1 & 0 & -l_z \\ 1 & 0 & l_z \\ -1 & 0 & -l_z \\ 0 & 1 & 0 \\ 0 & -1 & 0 \end{bmatrix}, \tag{21}$$

$$\begin{bmatrix} f_x^p \\ f_y^p \\ m_z^p \end{bmatrix} = \overline{\mathbf{R}}_\mathbf{a} \begin{bmatrix} f_4^p \\ f_5^p \\ f_6^p \end{bmatrix} = \overline{\mathbf{R}}_\mathbf{a} \left(\overline{k}_p + \overline{c}_p \frac{\mathrm{d}}{\mathrm{d}t} \right) \left(\begin{bmatrix} \hat{z}_4 \\ \hat{z}_5 \\ \hat{z}_6 \end{bmatrix} - \overline{\mathbf{R}}_\mathbf{b} \begin{bmatrix} \overline{x} \\ \overline{y} \\ \overline{\theta}_z \end{bmatrix} \right), \tag{22}$$

where $\overline{k}_p$ is the stiffness of the spring in the horizontal directions and $\overline{c}_p$ the damping constant of the damper in the horizontal directions.

It is found that the dynamics of the six modes can be treated separately, and, in addition, each mode for isolation table and middle table are represented in a similar form such as

$$m^\xi \ddot{\xi} = -k_s^\xi (\xi - \overline{\xi}) - k_i^\xi i^\xi - \left(k_3^\xi + c_3^\xi \frac{\mathrm{d}}{\mathrm{d}t} \right) (\xi - \hat{\xi}) + w^\xi, \tag{23}$$

$$\overline{m}^\xi \ddot{\overline{\xi}} = k_s^\xi (\xi - \overline{\xi}) + k_i^\xi i^\xi - \left(k_p^\xi + c_p^\xi \frac{\mathrm{d}}{\mathrm{d}t} \right) (\overline{\xi} - \hat{\xi}). \tag{24}$$

The variables and coefficients for each mode are defined as shown in Tables 1 and 2.

The developed system has six-degree-of-freedom motions (six modes). From Eq. (3), the zero-power controller of each mode is designed to have such dynamics as

$$I^\xi(s) = -\frac{s(\tilde{h}_2 s + \tilde{h}_1)}{s^2 + g_1 s + g_0} \xi(s) = -s q^\xi(s) \xi(s), \tag{25}$$

where

$$q^\xi(s) = -\frac{(\tilde{h}_2 s + \tilde{h}_1)}{s^2 + g_1 s + g_0}. \tag{26}$$

Table 1
Variables and coefficients for vertical modes.

	Z	Θ_x	Θ_y
ξ	z	θ_x	θ_y
$\overline{\xi}$	$\overline{z}$	$\overline{\theta}_x$	$\overline{\theta}_y$
$\hat{\xi}$	$\frac{\hat{z}_1+\hat{z}_2+\hat{z}_3+\hat{z}_4}{4}$	$\frac{\hat{z}_1-\hat{z}_2+\hat{z}_3-\hat{z}_4}{4}$	$\frac{\hat{z}_1+\hat{z}_2-\hat{z}_3-\hat{z}_4}{4}$
m^ξ	m	J_x	J_y
$\overline{m}^\xi$	$\overline{m}$	$\overline{J}_x$	$\overline{J}_y$
k_s^ξ	$4k_s$	$4k_s l_x$	$4k_s l_y$
k_i^ξ	k_i	$K_i l_x$	$K_i l_y$
I^ξ	$i_1+i_2+i_3+i_4$	$i_1-i_2+i_3-i_4$	$i_1+i_2-i_3-i_4$
k_p^ξ	$4k_p$	$4k_p l_x$	$4k_p l_y$
c_p^ξ	$4c_p$	$4c_p l_x$	$4c_p l_y$
w^ξ	f_z^d	m_x^d	m_y^d
k_3^ξ	$4k_3$	$4k_3 \overline{l}_x$	$4k_3 \overline{l}_y$
c_3^ξ	$4c_3$	$4c_3 \overline{l}_x$	$4c_3 \overline{l}_y$

Table 2
Variables and coefficients for horizontal modes.

	X	Y	Θ_z
ξ	x	y	θ_z
$\overline{\xi}$	$\overline{x}$	$\overline{y}$	$\overline{\theta}_z$
$\hat{\xi}$	$\frac{-\hat{z}_e+\hat{z}_f}{2}$	$\frac{-\hat{z}_a+\hat{z}_b-\hat{z}_c+\hat{z}_d}{4}$	$\frac{\hat{z}_a-\hat{z}_b-\hat{z}_c+\hat{z}_d}{4}$
m^{ξ}	m	m	J_z
$\overline{m}^{\xi}$	$\overline{m}$	$\overline{m}$	$\overline{J}_z$
k_s^{ξ}	$2\overline{k}_s$	$4\overline{k}_s$	$4\overline{k}_s l_z$
k_i^{ξ}	$\overline{k}_i$	$\overline{k}_i$	$\overline{k}_i l_z$
i^{ξ}	i_e-i_f	$i_a-i_b+i_c-i_d$	$i_a-i_b-i_c+i_d$
k_p^{ξ}	$2\overline{k}_p$	$4\overline{k}_p$	$4\overline{k}_p l_z$
c_p^{ξ}	$2\overline{c}_p$	$4\overline{c}_p$	$4\overline{c}_p l_z$
w^{ξ}	f_x^d	f_y^d	m_z^d
k_3^{ξ}	$2\overline{k}_3$	$4\overline{k}_3$	$4\overline{k}_3 \overline{l}_z$
c_3^{ξ}	$2\overline{c}_3$	$4\overline{c}_3$	$4\overline{c}_3 \overline{l}_z$

3.2. Response to direct disturbance

In the following analysis, it is assumed for simplicity that the initial values are zero and each Laplace-transformed variable is denoted by its capital. Therefore, the transfer function representation of the dynamics for isolation table and middle table described by Eqs. (23) and (24) can be written as

$$\Xi(s)=\frac{\tilde{k}_1(s)\tilde{k}_2(s)+\tilde{k}_2(s)\tilde{k}_3(s)+\tilde{k}_3(s)\tilde{t}_1(s)}{\tilde{t}_c(s)}\hat{\Xi}(s)+\frac{\tilde{t}_1(s)+\tilde{k}_2(s)}{\tilde{t}_c(s)}W^{\xi}(s), \tag{27}$$

and

$$\overline{\Xi}(s)=\frac{\tilde{k}_1(s)\tilde{k}_2(s)+\tilde{k}_1(s)\tilde{t}_2(s)+\tilde{k}_2(s)\tilde{k}_3(s)}{\tilde{t}_c(s)}\hat{\Xi}(s)+\frac{\tilde{k}_2(s)}{\tilde{t}_c(s)}W^{\xi}(s), \tag{28}$$

where

$$\tilde{t}_1(s)=\overline{m}^{\xi}s^2+c_p^{\xi}s+k_p^{\xi}, \tag{29}$$

$$\tilde{t}_2(s)=m^{\xi}s^2+c_3^{\xi}s+k_3^{\xi}, \tag{30}$$

$$\tilde{k}_1(s)=k_p^{\xi}+c_p^{\xi}s, \tag{31}$$

$$\tilde{k}_2(s)=k_i^{\xi}q^{\xi}(s)s-k_s^{\xi}, \tag{32}$$

$$\tilde{k}_3(s)=k_3^{\xi}+c_3^{\xi}s, \tag{33}$$

$$\tilde{t}_c(s)=\tilde{t}_1(s)\tilde{t}_2(s)+\tilde{k}_2(s)(\tilde{t}_1(s)+\tilde{t}_2(s)). \tag{34}$$

To estimate the stiffness for direct disturbance on the table, the direct disturbance W^{ξ} is assumed to be stepwise, that is

$$W^{\xi}=\frac{F_0}{s}\quad (\mathrm{F_0}:\mathrm{const}). \tag{35}$$

When the vibration of the floor is neglected ($\hat{\xi}=0$), the steady-state displacement of the table is obtained as

$$\frac{\xi(\infty)}{F_0}=\lim_{s\to 0}\frac{m^{\xi}s^2+(c_p^{\xi}+k_i^{\xi}c_2^{\xi}(s))s+k_p^{\xi}-k_s^{\xi}}{\tilde{t}_c(s)}=\frac{k_p^{\xi}-k_s^{\xi}}{k_3^{\xi}(k_p^{\xi}-k_s^{\xi})-k_p^{\xi}k_s^{\xi}} \tag{36}$$

when

$$k_p^{\xi}=k_s^{\xi}, \tag{37}$$

is satisfied in all modes, then

$$\frac{\xi(\infty)}{F_0}=0. \tag{38}$$

Therefore, the suspension system between the isolation table and the floor has zero-compliance to direct disturbances or infinite stiffness for any finite value of k_3. Eq. (38) shows that the suspension system between the isolation table and the

base has infinite stiffness statically, because there is no steady-state deflection even in the presence of stepwise disturbance acting on the table.

It should be noted that if k_2 (k_s in the zero-power control system) is not constant against load increment, Eq. (38) will not be realized in the end. In such a case, nonlinear compensator presented by Hoque et al. [22] can solve such problem.

4. Design and implementation of control system

The levitation of the isolation table and control of its motions consisted of two control approaches using two separate mode-based centralized controllers. One was controller for vertical motions, and the other was controller for horizontal motions. The sensors and actuators arrangement in and around the isolation table is shown in Fig. 4. For the developed system, there was redundancy in actuators, as more actuators were used to control motions both in the vertical and horizontal directions. Therefore, two mode-based centralized controllers were designed and implemented to control the 6-DOF motions (six modes). The block diagrams of the mode-based controllers are shown in Fig. 5. For each mode, an active zero-power controller (presented in Eq. (3)) was used. The control current of each mode was distributed to the respective actuators according to their positions. It should be noted that design of controller in the vertical direction is a challenging task as it includes stable levitation as well as motions control. The vertical motion controller was a four-channel MIMO system as there were four sensors and four actuators for controlling three modes. The horizontal motion controller was a six-channel MIMO system which included six sensors and six actuators for controlling other three modes. The schematic of a single-mode control vibration isolation and control system is delineated in Fig. 6. However, all the modes can be controlled by two controllers in a similar way. In designing the zero-power controller by Eq. (3), it is assumed that, $\omega_1=\omega_2=\omega$ and $\zeta_1=\zeta_2=\zeta$. The poles can be assigned arbitrarily by changing the values of ζ and ω. DS1103, the DSP produced by dSPACE, Germany, was used for the controller, and the control algorithm was implemented with MATLAB and Simulink. The sampling frequency was set at 10 kHz.

5. Experimental demonstrations

The levitation of the isolation table and control of its motions were carried out using the setup illustrated in Fig. 2. Several experiments have been conducted to demonstrate the feasibility of the developed vibration isolation and control system. First of all, zero-power control was realized between the isolation table and middle table for stable levitation. The positive and negative stiffness springs were, then, adjusted to satisfy Eq. (37). The stiffness could either be adjusted in the

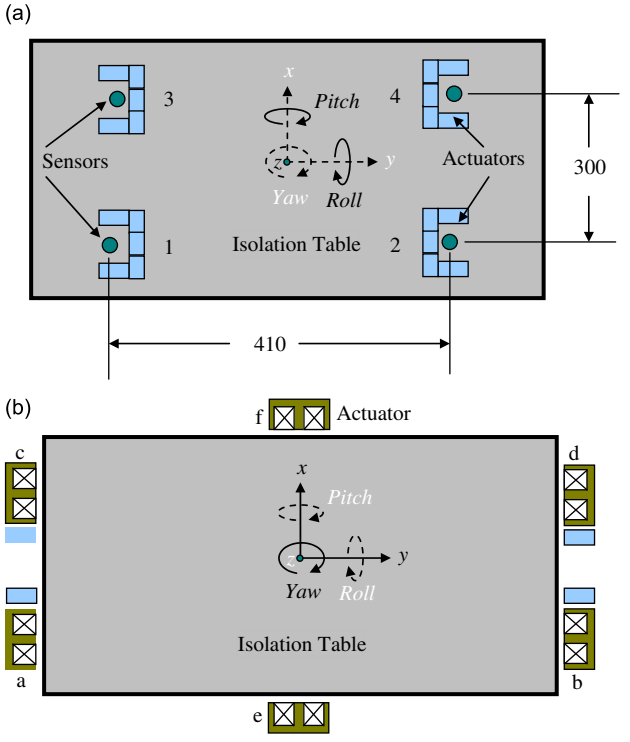

Fig. 4. Sensors and actuators arrangement in and around the isolation table (top view): (a) vertical motion control arrangement and (b) horizontal motion control arrangement. Sensors and actuators indicated by 1, 2, 3 and 4 are used for levitation and vertical motion control, and those indicated by a, b, c, d, e and f are used for horizontal motions control. Dimensions are in mm.

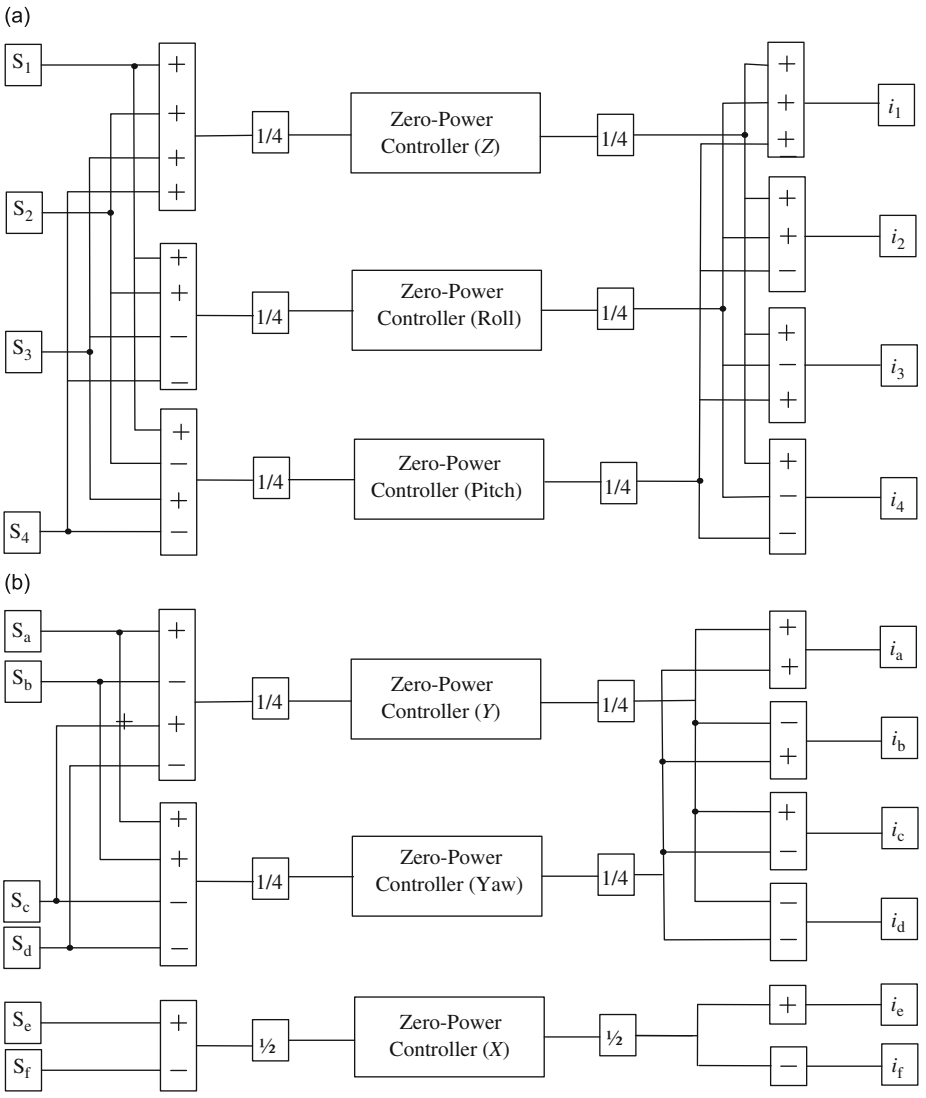

Fig. 5. Block diagram of the mode-based controllers: (a) for vertical motions and (b) for horizontal motions.

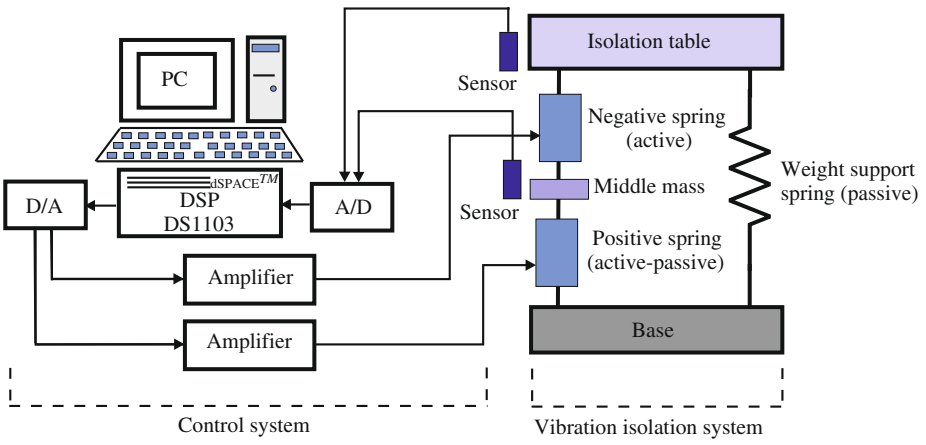

Fig. 6. Vibration isolation and control system of a single-mode motion control.

positive or negative stiffness part. In the former, PD control could be used in the electromagnets that were employed in parallel with the coil springs. In the latter, a PD control could be used in parallel with the zero-power control. For better performance, the latter was adopted in this experiment.

5.1. Static response of the system

Static direct disturbance was generated by putting stepwise static load on the isolation table. This experiment was conducted considering the viewpoint in the semiconductor manufacturing plant, where fabricated products move from table to table generating stepwise static direct disturbance.

The static response of the isolation table is illustrated in Fig. 7. First, static downward forces were put on the center of the isolation table to generate static direct disturbances in the z-direction, and the displacements of the isolation table and the middle table were measured. It is seen from the figure that zero-compliance to direct disturbance of the isolation table was realized up to 50 N while the position of middle table and the gap between table and middle table changes according to the increment of payloads. A high stiffness was realized between the base and table in this range which practically satisfied Eq. (38). Moreover, further experiments were conducted with the linearized zero-power controller [22]. It is clear that zero-compliance to direct disturbance was realized up to 90 N payloads with nonlinear compensation. The stiffness of the isolation system was increased to 960 N/mm, which was approximately 2.8 times more than that of without nonlinear control. The figure illustrates significant improvement in rejecting on-board-generated disturbances. Similar experiments were also carried out to measure the static response of the table to rotational motions by applying moment on the table. A typical rotational motion in the roll direction is shown in Fig. 8. It confirms that direct disturbance can be suppressed in the rotational motion, as it also realized zero-compliance to direct disturbances.

5.2. Dynamic response of the system

Dynamic direct disturbance to the table was generated by two voice coil motors attached to the base through a supplementary attachment. The dynamic performance of the isolation table was measured in the vertical direction as shown in Fig. 9. In this case, zero-power controller was designed by placing the pole at $\omega_1=\omega_2=\omega=2\pi\times 4$ [1/s] and $\zeta_1=\zeta_2=\zeta=0.8$. The isolation table was excited to produce sinusoidal disturbance force by the voice coil motors. The displacement of the table was measured by gap sensors, and the data was captured by a dynamic signal analyzer. It is

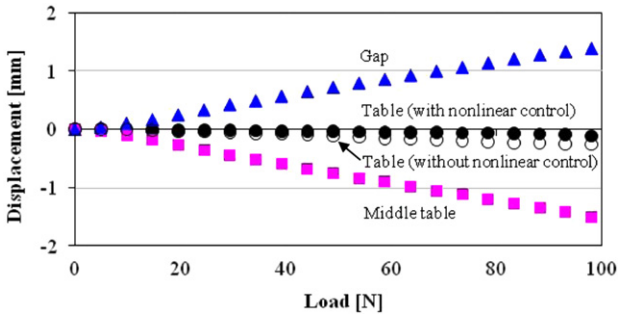

Fig. 7. Static response to direct disturbance for translational motion (Z).

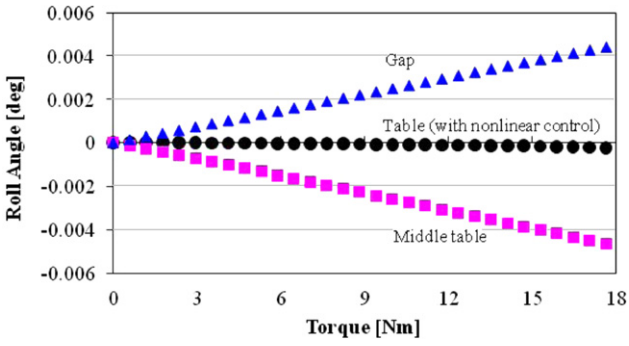

Fig. 8. Static response to direct disturbance for rotational motion by applying moment (roll mode, Θ_y).

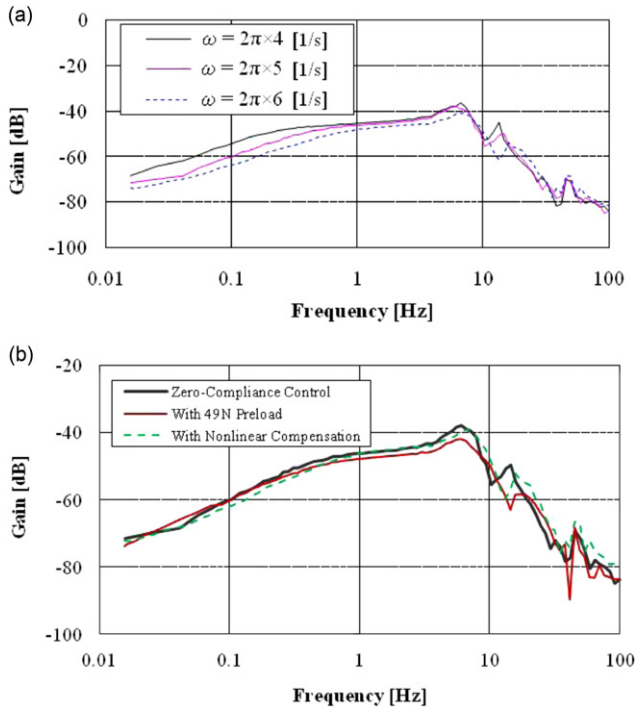

Fig. 9. Dynamic response of the isolation table to direct disturbance in the vertical translational direction: (a) effect of pole assignment and (b) effect of preload and nonlinear compensation.

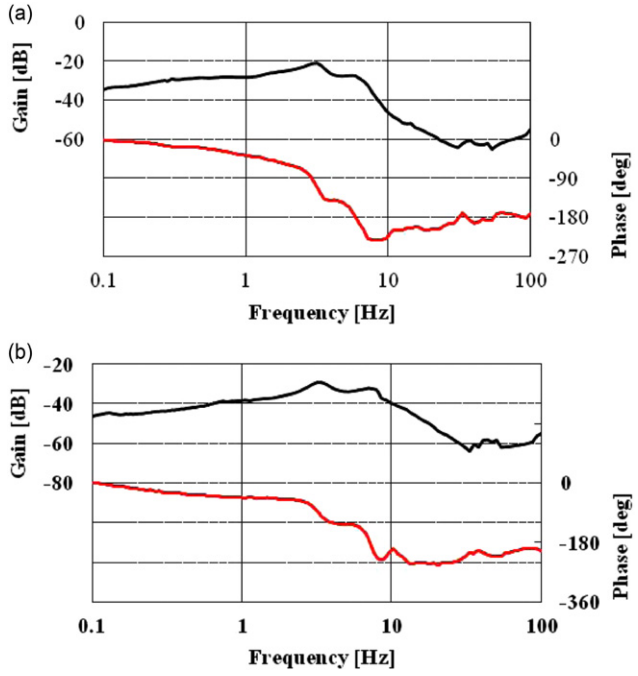

Fig. 10. Dynamic response of the isolation table in the horizontal directions: (a) translational motion (*Y*-mode) and (b) rotational motion (yaw mode).

found from Fig. 9(a) that the displacement of the isolation table is reduced at low frequency region below 1 Hz. The displacement of the isolation table at 0.015 Hz was -68 dB [mm/N]. It confirms that the developed system can generate high stiffness to static direct disturbance. Further investigation was conducted by assigning higher poles at ω=$2\pi \times 5$ [1/s] and ω=$2\pi \times 6$ [1/s] keeping damping parameter constant at $\zeta_1 = \zeta_2 = \zeta = 0.8$. The results also reveal that the displacement of the isolation was further reduced to -71 and -74 dB, respectively. It confirms that the dynamic performance of the

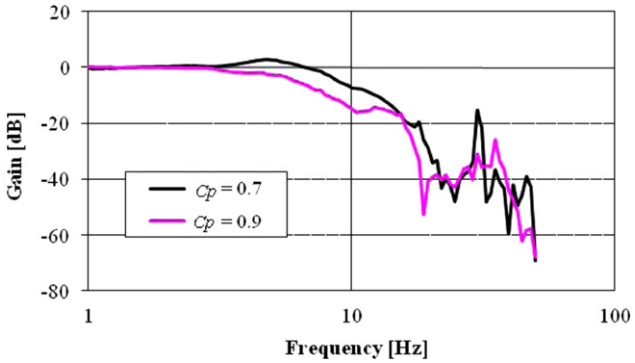

Fig. 11. Absolute transmissibility of the isolation table from base.

zero-power controller can be improved by assigning higher closed-loop poles of the feedback control system. Fig. 9(b) represents the dynamic performance of the table when static preload and nonlinear compensation of the zero-power controller were introduced. It also demonstrates that direct disturbance rejection performances were not worsened even though preload or nonlinear zero-power controls was introduced. It demonstrates the idea that the developed isolation system can support any rotating machine loaded on the table which even has periodic excitation.

The characteristics of the isolation table were further investigated by measuring the response of the table to direct disturbance in the horizontal directions as shown in Fig. 10. In this case, four voice coil motors were used to excite the isolation table along the horizontal translational and rotational directions. The results show the dynamic response of the isolation table when the table was excited along *Y* and yaw modes. The response of the table to direct dynamic disturbance was captured by dynamic signal analyzer. The results justify that the displacements of the table to direct disturbance in the horizontal rotational motions were also low at the low frequency regions. The results confirmed that the high stiffness of the isolation table was realized against disturbing forces in the motions associated with horizontal directions.

5.3. Response of the system to ground vibrations

Fig. 11 shows the absolute transmissibility of the isolation table from the base of the developed system. In this case, the base of the system was sinusoidally excited in the vertical direction by a high-powered pneumatic actuator attached to the base, and the displacement transfer function (transmissibility) of the isolation table was measured from the base. The base displacement in the vertical direction was considered as input, and the output signal was the displacement of the isolation table. The damping coefficient (c_p) between the base and the middle table played an important role to suppress the resonance peak. The figure shows that the resonant peak was almost suppressed when c_p was chosen as 0.9. It is clear from the figure that the developed system can effectively isolate the floor vibration that transmitted through the suspensions, such as active–passive positive suspensions and active zero-power controlled magnetic suspension.

6. Conclusions

A six-axis vibration isolation system has been developed using active zero-power controlled magnetic suspension. The system was further reinforced by introducing a passive weight support mechanism in order to simplify the complex magnetic suspension system, and to support huge isolation table or large payloads on the table. In this system, two separate mode-based centralized controllers were designed to control the six motions, associated with the vertical and horizontal directions, actively. Although the control system design exhibited good suspension and motion control of the isolation table, there were redundant actuators both in the vertical and horizontal directions. Therefore, the research can be extended to develop a multi-degree-of-freedom vibration isolation system combining multiple vibration isolation modules. Such a vibration isolation module can be controlled by a simple local (decentralized) controller with a single actuator. Therefore, the number of motions to be controlled would be equal to the number of actuators.

The mathematical model of the system was completely presented, and it was analytically established that any mode of the system could have infinite stiffness to static direct disturbances when positive and negative stiffness are equal in magnitude. This characteristic was experimentally verified both for translational and rotational motions. The feasibility of supporting large isolation table, inclusion of nonlinear compensation, and suppressing the effects of direct disturbance were verified by experimental study both statically and dynamically. It is also verified that the performance of the zero-power controller could be improved by selecting higher closed-loop poles of the feedback controller. It can be noted that direct disturbance rejection, moreover, could well be improved by incorporating a feedforward controller with the feedback control. The transmissibility characteristics of the developed system demonstrated good ground vibration isolation performances as well. It is confirmed that the ground vibration isolation performance, however, was not worsened even though high stiffness was generated to reject the direct disturbances. It is noteworthy that the dynamic

performance of the system depends both on the control parameters as well as the physical parameters of the system. Therefore, an integrated optimal design of mechanism and control parameters are vital to improve the dynamic performances more effectively.

Acknowledgments

The authors gratefully acknowledge the financial support made available from the Ministry of Education, Culture, Sports, Science and Technology of Japan, a Grant-in-Aid for Scientific Research (B), and a Grant-in-Aid from Japan Society for the Promotion of Science (JSPS) (JSPS Grant no. 20.08380).

References

[1] E.I. Rivin, *Passive Vibration Isolation*, ASME Press, New York, USA, 2003.
[2] C.M. Harris, *Shock and Vibration Handbook*, fouth ed., McGraw Hill, New York, 1996.
[3] C.R. Fuller, S.J. Elliott, P.A. Nelson, *Active Control of Vibration*, Academic Press, New York, 1997.
[4] L. Benassi, S.J. Elliot, P. Gardonio, Active vibration isolation using an inertial actuator with local force feedback control, *Journal of Sound and Vibration* 276 (3) (2004) 157–179.
[5] M. Yasuda, M. Ikeda, Double-active control of microvibration isolation systems to improve performances (application of two-degree-of-freedom control), *Transactions of the Japan Society of Mechanical Engineers, Series C* 59 (562) (1993) 1694–1701 (in Japanese).
[6] H. Yoshioka, Y. Takahashi, K. Katayama, T. Imazawa, N. Murai, An active microvibration isolation system for hi-tech manufacturing facilities, *ASME Journal of Vibration and Acoustics* 123 (2001) 269–275.
[7] M. Yasuda, T. Osaka, M. Ikeda, Feed forward control of a vibration isolation system for disturbance suppression, in: Proceedings of the 35th IEEE Conference on Decision and Control, Kobe, Japan, 1996, pp. 1229–1233.
[8] K. Watanabe, S. Hara, Y. Kanemitsu, T. Haga, K. Yano, T. Mizuno, Combination of H^{∞} and PI control for an electromagnetically levitated vibration isolation system, in: Proceedings of the 35th IEEE Conference on Decision and Control, Kobe, Japan, 1996, pp. 1223–1228.
[9] S. Daley, J. Hatonen, D.H. Owens, Active vibration isolation in a "smart spring" mount using a repetitive control approach, *Control Engineering Practice* 14 (2006) 991–997.
[10] W.H. Zhu, B. Tryggvason, J.C. Piedboeuf, On active acceleration control of vibration isolation systems, *Control Engineering Practice* 14 (8) (2006) 863–873.
[11] T. Sato, D.L. Trumper, A novel single degree-of-freedom active vibration isolation system, in: Proceedings of the 8th International Symposium on Magnetic Bearing, Japan, August 26–28, 2002, pp. 193–198.
[12] T. Mizuno, T. Toumiya, M. Takasaki, Vibration isolation system using negative stiffness, *JSME International Journal, Series C* 46 (3) (2003) 807–812.
[13] M.E. Hoque, M. Takasaki, Y. Ishino, T. Mizuno, Design of a mode-based controller for 3-dof vibration isolation system, in: Proceedings of the 2004 IEEE Conference on Robotics, Automation and Mechatronics, Singapore, December 1–3, 2004, pp. 478–483.
[14] M.E. Hoque, M. Takasaki, Y. Ishino, T. Mizuno, Development of a three-axis active vibration isolator using zero-power control, *IEEE/ASME Transactions on Mechatronics* 11 (4) (2006) 462–470.
[15] M. Morishita, T. Azukizawa, S. Kanda, N. Tamura, T. Yokoyama, A new maglev system for magnetically levitated carrier system, *IEEE Transaction on Vehicular Technology* 38 (4) (1989) 230–236.
[16] A.V. Sabnis, J.B. Dendy, F.M. Schmitt, Magnetically suspended large momentum wheel, *Journal of Spacecraft* 12 (1975) 420–427.
[17] T. Mizuno, Y. Takemori, A transfer-function approach to the analysis and design of zero-power controllers for magnetic suspension system, *Electrical Engineering in Japan* 141 (2) (2002) 933–940.
[18] T. Mizuno, M. Takasaki, D. Kishita, K. Hirakawa, Vibration isolation system combining zero-power magnetic suspension with springs, *Control Engineering Practice* 15 (2) (2007) 187–196.
[19] T. Mizuno, D. Kishita, M.E. Hoque, M. Takasaki, Y. Ishino, Vibration isolation system using zero-power magnetic suspension with a weight suspension mechanism, in: CD-ROM Proceedings of the 16th IFAC World Congress, Prague, Czech Republic, July 4–8, 2005, paper ID. 02625.
[20] T. Mizuno, M.E. Hoque, M. Takasaki, Y. Ishino, Development of a six-axis hybrid vibration isolation system using zero-power control, in: CD-ROM Proceedings of the 45th IEEE Conference on Decision and Control, USA, December 13–15, 2006, pp. 6531–6536.
[21] D.L. Platus, Negative-stiffness-mechanism vibration isolation system, in: Proceedings of the SPIE, Vibration Control in Microelectronics, Optics, and Metrology, 1991, Vol. 1619, pp. 44–54.
[22] M.E. Hoque, T. Kamiya, T. Mizuno, A nonlinear compensator for zero-power control and its application to vibration isolation system, in: Proceedings of the IEEE/ASME International Conference on Mechatronic and Embedded Systems and Application (IDETC/CIE 2005), California, USA, September 2005, paper no. DETC2005-85175.